doi: 10.4149/gpb_2025020

WTAP regulates DDX3Y mRNA *via* m6A modification to promote high glucose-induced podocytes injury and diabetic nephropathy progression

Guanxi Li[1], Huijuan Zeng[1], Guojia Ru[1], Fang Yin[1], Siyi Liu[1] and Jie He[1]

[1] *The Second Department of Nephrology, The First Affiliated Hospital of Kunming Medical University, Kunming, China*

Abstract. Diabetic nephropathy (DN) is a major complication of diabetes, imposing substantial socioeconomic and public health challenges. N6-methyladenosine (m6A) modification, a prevalent epigenetic mechanism, influences cellular processes and disease progression. Wilms' tumor 1-associating protein (WTAP), an m6A methyltransferase subunit, was investigated for its role in DN. Bioinformatics identified differentially expressed genes in DN, and a high glucose (HG)-induced podocyte model was established to mimic DN *in vitro*. Techniques like Western blot, CCK-8, ELISA, flow cytometry, and TUNEL evaluated protein expression, cell viability, inflammation, oxidative stress, and apoptosis. SRAMP predicted m6A sites in DDX3Y mRNA, validated by MeRIP, while xenograft models confirmed *in vivo* effects. DDX3Y expression was elevated in DN and HG-induced podocytes, and sh-DDX3Y attenuated HG-induced injury. WTAP promoted DDX3Y mRNA stability *via* m6A methylation, exacerbating podocyte dysfunction. In diabetic mice, WTAP modulated DDX3Y to induce renal insufficiency and histopathological damage. Collectively, WTAP regulates DDX3Y *via* m6A methylation to promote HG-induced podocyte injury and DN progression.

Key words: Diabetic nephropathy — Podocytes — m6A — WTAP — DDX3Y

Introduction

Diabetic nephropathy (DN) is caused by proteinuria and a gradual reduction in glomerular filtration rate (GFR) due to prolonged diabetes (Sagoo and Gnudi 2020). Over the years, DN damages the renal filtration system and impairs the kidneys' ability to function properly, preventing them from removing wastes and excess fluids from the body and, in more serious cases, leading to renal failure, also known as end-stage renal disease (ESRD) (Samsu 2021; Qiu et al. 2023). Once ESRD develops, treatment is often trickier than other kidney diseases (Queeley and Campbell 2018). The incidence of diabetic nephropathy is also on the rise in China and has become the second leading cause of end-stage renal disease after glomerulonephritis (Zhang and Kong 2020). Early treatment can prevent or delay the onset of the disease and reduce complications (Elendu et al. 2023).

N6-methyladenosine (m6A) is a dynamic and reversible modification catalyzed by methyltransferases and demethylases, as well as by binding proteins, with important regulatory functions in a wide range of cellular processes and disease pathologies (He et al. 2019; Jiang et al. 2021). In past decades, RNA detection technology has developed. As a result, the exploration of the biological function of m6A modification has become a cutting-edge hotspot in the field of RNA (Zhang et al. 2021). A variety of studies have explored the roles of m6A modification in the progression of DN by modifying different target genes (Li et al. 2022; Qin et al. 2023; Fu et al. 2024). Besides, the search for more targets is highly beneficial for disease understanding and control. The process of m6A methylation is mediated by the methyltransferase complex (MTC), which consists of several enzymes and proteins (Huang et al. 2020). Among them, methyltransferase-like pro-

Electronic supplementary material. The online version of this article (doi: 10.4149/gpb_2025020) contains Supplementary material.

Correspondence to: Jie He, The Second Department of Nephrology, The First Affiliated Hospital of Kunming Medical University, No. 295, Xichang Road, Kunming 650000, China
E-mail: hejie402312@163.com

© The Authors 2025. This is an **open access** article under the terms of the Creative Commons Attribution-NonCommercial 4.0 International License (https://creativecommons.org/licenses/by-nc/4.0/), which permits non-commercial use, distribution, and reproduction in any medium, provided the original work is properly cited.

tein (METTL) 3 is an important catalytic subunit (Zeng and Huang 2020), METTL14 has no methyltransferase activity by itself and mainly acts as a protein conformational activator of METTL3 enzyme activity, helping METTL3 to recognize the substrate (Dou et al. 2023). METTL16 is involved in catalytic m6A modification (Su et al. 2022), and Wilms' tumor 1-associating protein (WTAP) binds directly to METTL3, ensuring the localization of the METTL3-METTL14 heterodimer and improving catalytic activity (Horiuchi et al. 2021). A recent study has illustrated that WTAP and METTL14 played a key role in DN by mediating m6A modification in renal tubular epithelial cells (Fu et al. 2024). Besides, it was proved that m6A modification of NLRP3 mediated by WTAP contributed to pyroptosis and inflammation in human renal tubular epithelial cells (Lan et al. 2022). During the process of DN, damage to the podocytes has a strong influence on the onset and development of proteinuria, which can lead to exacerbation of DN and the eventual development of ESRD. Therefore, more and more scholars consider DN as a 'podocytosis' (Zhang et al. 2020). It has been found in the literature that high glucose stimulation leads to epithelial-to-mesenchymal trans-differentiation of podocytes.

The protein encoded by the DDX3Y gene belongs to the Asp-Glu-Ala-Asp (DEAD)-box RNA helicase family, containing nine conserved motifs that are associated with ATP binding, hydrolysis, RNA binding and intramolecular interaction establishment (Lacroix et al. 2023). Research indicated that the DDX family often displayed altered expression in tumor tissues, which was a key factor in the genesis and progression of tumors (Li et al. 2024). This family contributes to processes such as tumor cell proliferation, apoptosis, cell cycle, invasion, metastasis and metabolism, which could serve as novel molecular markers for tumors and also provide new potential molecular targets for therapeutic approaches in tumor treatment (Wu et al. 2024). However, its mechanism of action in DN is currently not well elucidated. Therefore, the goal of this study was to elucidate the role of WTAP in podocytes affected by DN and to understand the significance of the regulatory relationship between WTAP and DDX3Y in the DN process, which may provide a new clue for diagnosis of DN.

Materials and Methods

Clinical samples

32 blood samples of DN patients were obtained from the First Affiliated Hospital of Kunming Medical University. 36 control samples were obtained from healthy volunteers. This study received approval from the ethics committee of the First Affiliated Hospital of Kunming Medical University and was conducted in accordance with the principles of the Declaration of Helsinki. Before the study began, all participating patients were informed about the use of their blood samples and all provided their informed consent.

Cell culture and treatment

The conditionally immortalized human podocyte cell lines were obtained from Sunncell (Wuhan, China) and cultured at 33°C in RPMI-1640 medium (Sigma-Aldrich, St. Louis, MO, USA) containing 10% fetal bovine serum (FBS) (Gibco, Grand Island, NY, USA), 1% penicillin/streptomycin (Invitrogen, Carlsbad, CA, USA) and 1× insulin-transferrin-selenium (ITS) (Beyotime, Shanghai, China) for proliferation. Cells were cultured in the complete RPMI-1640 medium without ITS at 37°C for 2 weeks for differentiation. The cells were subsequently separated into two groups: in the normal glucose (NG) group, cells were treated with normal glucose (5 mmol/l), in the high glucose (HG) group, cells were stimulated with 30 mmol/l glucose. Each group was stimulated by glucose for 48 hours.

Bioinformatics analysis

To examine the expression of DDX3Y in DN, the GEO database (https://www.ncbi.nlm.nih.gov/geo/query/acc.cgi?acc=GSE154881) was applied. Genes differentially expressed in the blood of 5 healthy donors and 4 DN patients in the GSE154881 were screened and analyzed.

Quantitative real-time polymerase chain reaction (qRT-PCR)

The mRNA level in clinical samples and cells was monitored by qRT-PCR assay. The RNA samples were obtained from blood samples and podocytes using Trizol reagent (Thermo Fisher Scientific, Waltham, MA, USA). Then, the concentrations of RNA were determined using NanoDrop 2000c (Thermo Fisher Scientific). The cDNA was generated using Transcriptor First Strand cDNA Synthesis Kit (Roche, Vilvoord, Brussels, Belgium). The qRT-PCR reaction was then performed using Real-Time PCR Detection System (Bio-Rad, Shanghai, China) with the SYBR Green Realtime PCR Master Mix (Toyobo Co., Osaka, Japan). All specific primers used in this article were synthesized by Songon (Shanghai, China), and the sequences of primers are listed in Table 1.

Western blot analysis

In order to analyze the protein expression level in podocytes, the Western blot was utilized. The proteins from cells or tissues were extracted using RIPA Lysis and Extraction Buffer (Thermo Fisher Scientific, Waltham, MA, USA). Then, the sodium dodecyl sulfate-polyacrylamide gel electrophoresis (SDS-PAGE) was conducted to separate protein samples.

Next, the proteins were transferred onto the PVDF membrane (GE Healthcare, Piscataway, NJ, USA) for blotting analysis. The membrane was blocked using 5% skimmed milk at 4°C overnight, after which, the membrane was incubated with primary antibodies against DDX3Y (DDX3Y Polyclonal antibody (1:600, Cat: 14041-1-AP, Proteintech, Wuhan, China), β-actin (Beta Actin Monoclonal antibody (1:10000, Cat: 66009-1-Ig, Proteintech) and WTAP (WTAP Polyclonal antibody (1:8000, Cat: 10200-1-AP, Proteintech) at room temperature for 1.5 h, followed by incubating with anti-mouse or anti-rabbit horseradish peroxidase (HRP)-conjugated antibodies (1:100000/1:1000, Cat: SA00001-1 /SA00001-2, Proteintech). Additionally, RapidStep ECL Reagent (Millipore Corp., Billerica, MA, United States) was utilized for visualizing the protein bands and observing the chemiluminescence intensity. Finally, the results were analyzed using ImageJ software (β-actin was used as an internal reference).

Cell transfection

shRNAs were designed by GeneChem (Shanghai, China), and the overexpression vector of DDX3Y (oe-DDX3Y) was constructed using pcDNA 3.1 (Invitrogen). Podocytes were transfected with shRNA targeting DDX3Y (sh-DDX3Y#1/2/3) or WTAP (sh-WTAP#1/2/3) or oe-DDX3Y using Lipofectamine 2000 (Invitrogen) in accordance with the instructions provided by the manufacturer.

Cell viability assay

Cell Counting Kit-8 (CCK-8; Dojindo, Kumamoto, Japan) was utilized for the analysis of cell viability. After digestion and counting, the podocytes were inoculated in 96-well plates at a density of 5×10^3 *per* well. After 0, 12, 24, and 48 h of culturing at 37°C, cells in each well were treated with 10 μl CCK-8 solution (Dojundo) for an extra 1 h at 37°C. Then, 150 μl DMSO was added, and cell viability was examined by detecting the absorbance at 450 nm using a spectrophotometer (Thermo Fisher Scientific).

Enzyme-Linked Immunosorbent Assay (ELISA)

ELISA was performed to detect inflammatory factors in podocytes or serum of experimental mice. The levels of IL-1β, TNF-α and IL-6 were respectively measured using Mouse/Human IL-1β ELISA Kit (Beyotime), Mouse/Human TNF-α ELISA Kit (Beyotime), Mouse/Human IL-6 ELISA Kit (Beyotime). All procedures were carried out following the instructions. In brief, the samples, biotin-labeled antibody, and enzyme-conjugate HRP were added according to the instructions provided in the kit, and the absorbance value at 450 nm was read by the microplate reader after color development using TMB. Finally, the concentration was calculated on the basis of the standard curve.

Table 1. Primers sequences used for qRT-PCR

	Primers for PCR (5'–3')	
DDX3Y	F:	TCGCTCAGGAAAAAGCCCAA
	R:	CCCAGGTTTCCTACACGTCC
WTAP	F:	GCTTCTGCCTGGAGAGGATT
	R:	GTGTACTTGCCCTCCAAAGC
β-actin	F:	CTTCGCGGGCGACGAT
	R:	CCACATAGGAATCCTTCTGACC

F, forward; R, reverse.

Measurement of intracellular ROS levels

The oxidative stress of podocytes in different groups was analyzed by detecting intracellular ROS levels. The Reactive Oxygen Species Assay Kit (Beyotime) was utilized in this process, and the procedures were carried out in conformity with the manufacturer's protocols. 2',7'-dichlorodihydrofluorescein diacetate (DCFH-DA) was incubated with cells in each group at 37°C for 20 min. Then, the ROS levels were quantified using flow cytometry (FACScan; BD Biosciences, San Jose, CA, USA).

Flow cytometry analysis

Cell apoptosis was monitored by flow cytometry. This assay was performed using the Annexin V-FITC/PI cell apoptosis analysis kit (Solarbio, Beijing, China). All concrete steps were conducted by the instructions offered by the manufacturer. Briefly, podocytes were digested and collected into centrifuge tubes. Then, 1× binding buffer was used to resuspend the cells, adjusting the cell concentration to $1–5\times10^6$/ml. Next, 100 μl of the cell suspension was aspirated into a 5 ml FACS tube and 5 μl of AnnexinV/FITC was used to mix with the cells and incubated for 5 min at room temperature away from light. Afterward, 5 μl of propidium iodide solution (PI) and 400 μl of PBS were added, and the cells were immediately subjected to flow cytometry (Agilent, Beijing, China).

Terminal deoxynucleotidyl transferase dUTP nick-end labeling (TUNEL) staining assay

For further estimating the DNA fragmentation in apoptotic cells of tissues and podocytes, the TUNEL assay was employed. One-step TUNEL In Situ Apoptosis Kit (Elabscience, Wuhan, China) was used for this assay in accordance with the manufacturer's protocols. First, 4% paraformaldehyde (Beyotime) was used to fix cell slides at 4°C for 2 h. Then, 0.2% TritonX-100 (Beyotime) was used for permeation at

37°C for 10 min. Next, cells were incubated with DNase I working solution at 37°C for 15 min. After incubating with TdT Equilibration Buffer and Labeling Solution at 37°C away from light, nuclei were stained with DAPI working solution. Finally, fluorescent signals produced by apoptotic cells were observed using fluorescence microscopy. As for the detection of apoptosis in mouse kidney tissue cells in the *in vivo* experiments, the procedure was basically the same as described above, but the fluorescent markers used in these two experiments were different.

MeRIP-qPCR assay

MeRIP-qPCR was performed to examine m6A methylation levels in HG-induced podocytes. Briefly, the total RNA extracted from cells was first purified using the Hieff NGS® mRNA Isolation Master Kit (Yeasen, Shanghai, China). 1/10 of poly (A) mRNA sample was used as input control temporarily placed at −80°C. Next, Pierce™ Protein A/G Magnetic Beads (Thermo Scientific) were prepared for coupling antibodies. The beads were incubated with m6A antibody or Rabbit IgG antibody at 4°C for 2 h using Vertical mixer (Thermo Fisher Scientific). After that, purified RNA was mixed with antibody-conjugated beads and 1× immunoprecipitation (IP) buffer containing RNase inhibitors. Subsequently, proteinase K was added to the mixture for digestion. Finally, the RNA in the input sample and the above mixture were precipitated in a RNase-free centrifuge tube using glycogen, sodium acetate and ethanol at −80°C. The next day, qPCR was applied to calculate the enrichment, and m6A levels in each group were calculated by normalizing to the input.

Measurement of mRNA stability

0.2 mmol/l actinomycin D (Sigma-Aldrich, St. Louis, MO, USA) was used to treat podocytes in each group. The cells treated with actinomycin D for 0, 3, 6 and 12 h were collected. Then, qRT-PCR was applied for the determination of quantitated mRNA levels.

Establishment of xenograft models

All animal experiments received approval from the First Affiliated Hospital of Kunming Medical University Ethics Committee, and all procedures were performed according to established International Guiding Principles for Animal Research. db/m and db/db mice were procured from Junke Biology Co., LTD (Nanjing, China). The mice were housed in proper cages kept at 24°C and 70% humidity and the feeding was strictly in accordance with the company's website requirements. To perform the experiment, the mice were randomly allocated into 3 groups (6 mice/group): db/db, db/db+sh-WTAP, and db/db+sh-WTAP+oe-DDX3Y. After 7 days of acclimatization, podocytes treated with different conditions were mixed with serum-free medium and were injected into the mice through the tail vein. One month after the injection of the cells, blood and urine samples were collected from each group of mice for assays, and the mice were anesthetized and sacrificed, and their kidney tissues were dissected out for subsequent analysis.

Tissue staining analysis

In order to observe the changes in renal tissue in different groups of mice, two staining methods were used for the staining of obtained tissue samples. The fresh kidney tissues were first fixed using 4% paraformaldehyde, dehydration was then carried out using a range of different concentrations of anhydrous ethanol. Next, the tissues were embedded in paraffin, and then, the tissues were thinly sliced. For hematoxylin-eosin (HE) staining, hematoxylin was first added to the sections for five minutes. After rinsing, they were differentiated using 1% ethanol hydrochloride. Then, a drop of 0.5% eosin stain was applied to the sections for 10–15 s. After dehydration and treatment with xylene, a drop of neutral gum was added to the tissues and the slides were covered. 24 h later, the tissues were photographed under a microscope. As for Periodic Acid-Schiff (PAS) staining, the basic procedure was the same as for HE staining, tissues were oxidized using periodic acid for 5 min before staining began, then, the Schiff reagent was added to the slices for 10 min, and hematoxylin was used for nuclear staining. Finally, Scott TapWater/Bluing was used for rebluing.

Measurement of renal tissue injury related indicators

To further determine the renal tissue damage, some indicators related to kidney damage were tested. First, the levels of BUN and Scr in serum were measured using Urea (BUN) Colorimetric Assay Kit (Urease Method) (Elabscience) and Mouse Serum Creatinine (S-Cr) ELISA Kit (Yaji Biological, Shanghai, China). In addition, the urine protein level was detected using Urine Protein Colorimetric Assay Kit (Elabscience). All experimental steps were carried out following the instructions provided by the manufacturer.

Statistical analysis

GraphPad Prism 8.0.1 software was utilized for data analysis, and cell experiments were independently performed 3 times. The data were presented as mean ± standard deviation (SD), and Student's *t*-test and one-way ANOVA followed by Tukey's test were employed for statistical analysis of differences in two or more groups. Additionally, Receiver Operating Characteristic (ROC) curve analysis in GraphPad

Prism was conducted to calculate the area under the curve (AUC), evaluating diagnostic efficiency. Pearson's correlation analysis was applied to assess the correlation between DDX3Y and WTAP mRNA levels. $p < 0.05$ was considered statistically significant.

Results

DDX3Y was highly expressed in DN and HG-induced podocytes

Differentially expressed genes in the blood of 5 healthy donors and 4 DN patients were presented by the GEO database (GSE154881). Among them, 3 up-regulated genes (ZFY, DDX3Y, and UTY) and 3 down-regulated genes (HBG1, HBG2, and CD177) were found in the blood of DN patients compared to healthy individuals (Fig. 1A,B). To validate these findings in relevant cells, we examined the mRNA levels of these 6 genes in normal podocytes and HG-induced podocytes (Fig. 1C), among which, DDX3Y was strikingly elevated in HG-induced podocytes. To further explore DDX3Y's expression in a more clinically relevant context, qRT-PCR was applied. The mRNA levels in the control group ($n = 36$) and HG group ($n = 32$) were displayed in Figure 1D. Besides, the ROC curve was used to analyze the diagnostic value where the cut-off value was 1.395 (Fig. 1E). At last, the protein levels of DDX3Y were

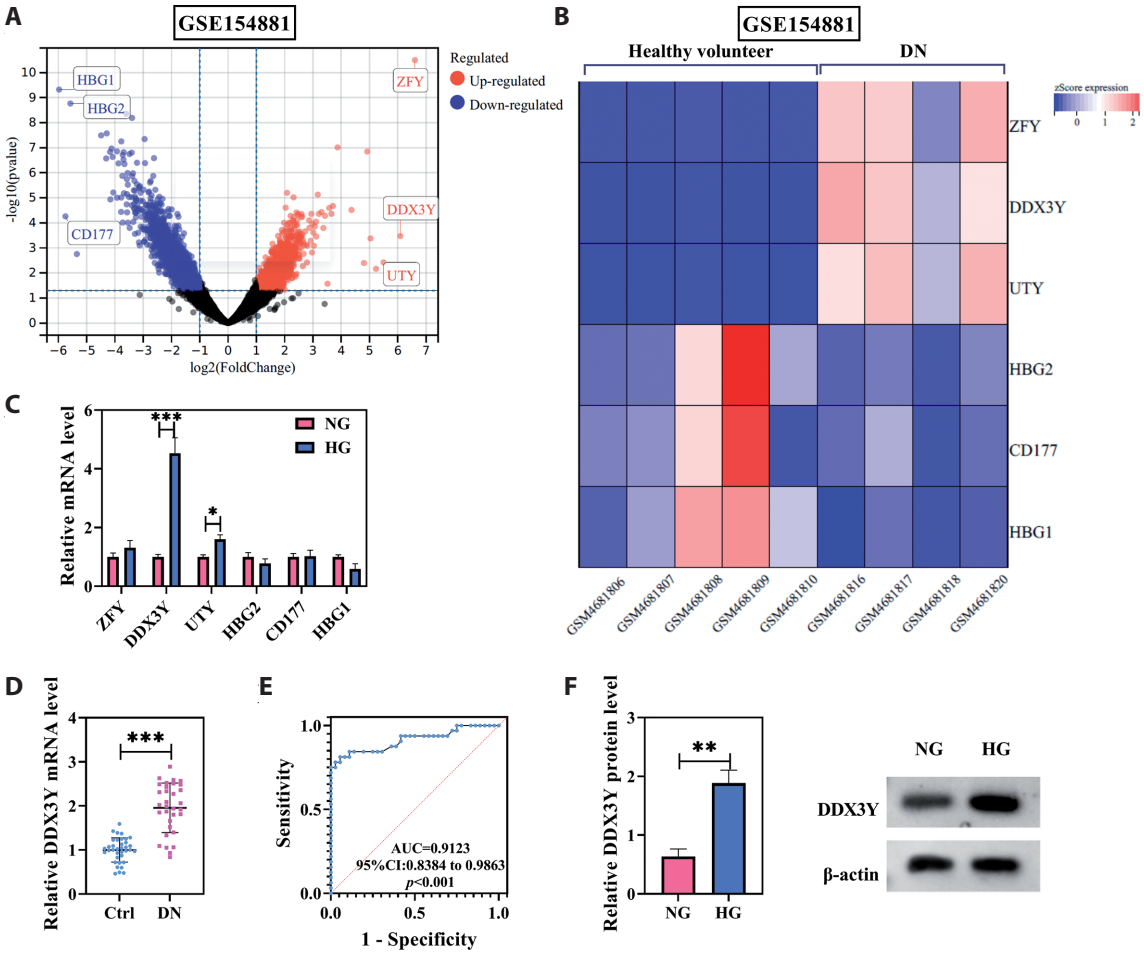

Figure 1. DDX3Y is elevated in DN and HG-induced podocytes. **A.** The up-regulated and down-regulated genes in the blood samples from healthy individuals and DN patients according to the data from the GEO dataset (GSE154881) were presented by a volcano plot. **B.** Heatmap showed the TOP 3 up-regulated or down-regulated genes in samples of 5 healthy volunteers and 4 DN patients based on the GEO (GES154881) dataset. **C.** qRT-PCR was applied to evaluate the mRNA level of TOP 3 up-regulated or down-regulated genes in NG- and HG-induced podocytes. **D.** The mRNA levels of DDX3Y in tissues of 36 healthy control (Ctrl) and 32 DN patients were detected by qRT-PCR. **E.** ROC curves were applied to analyze the diagnostic value (cut-off value = 1.395). **F.** DDX3Y protein expression levels in NG- and HG-induced podocytes were tested by Western blot. * $p < 0.05$, ** $p < 0.01$, *** $p < 0.001$.

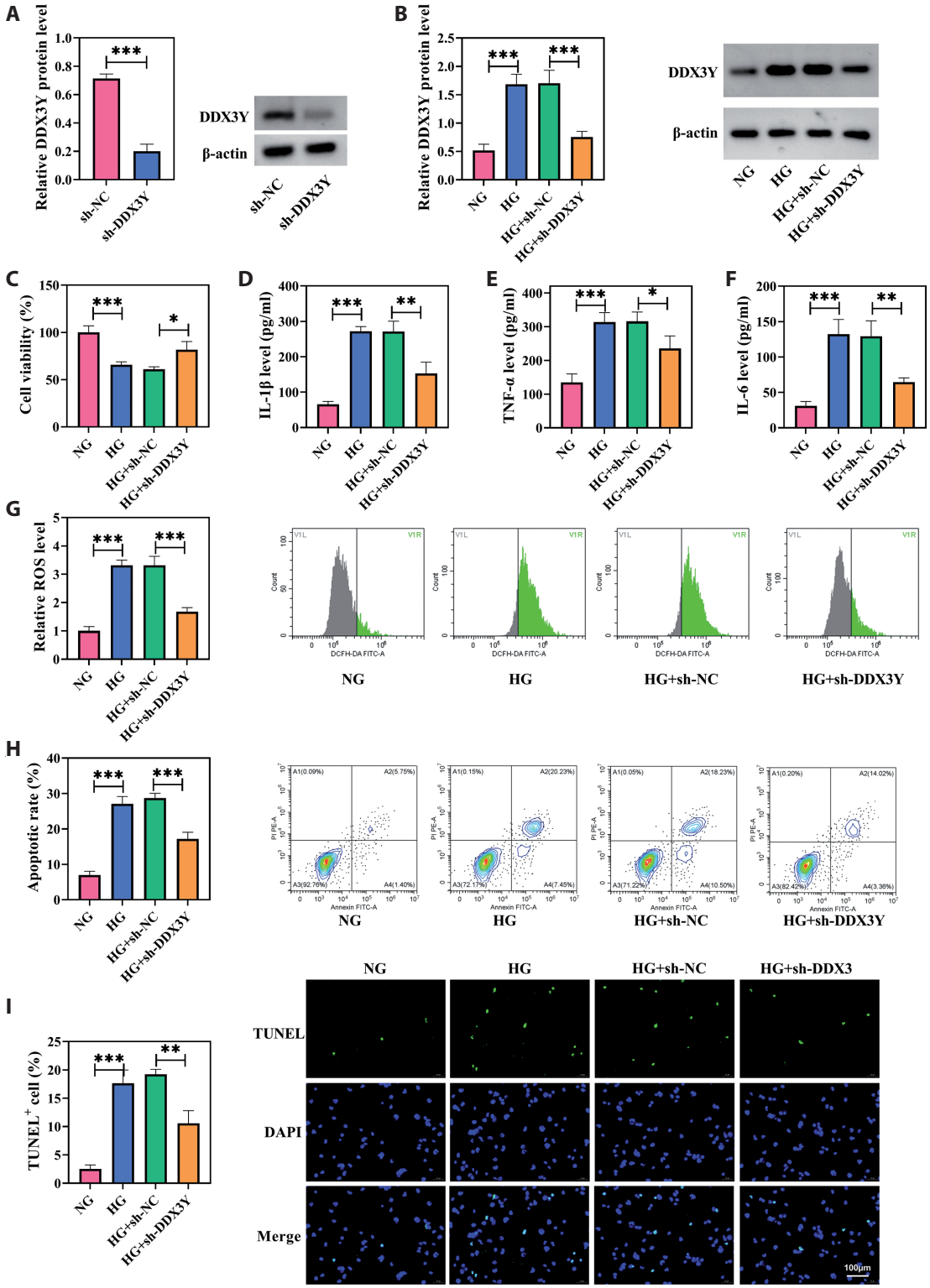

Figure 2. Silencing DDX3Y inhibits HG-induced cell injury in podocytes. Podocytes were transfected with sh-NC and sh-DDX3Y. **A,B.** DDX3Y protein level was detected using Western blot. **C.** CCK-8 assay was applied to monitor the cell viability of podocytes. The levels of IL-1β **(D)**, TNF-α **(E)** and IL-6 **(F)** were respectively measured by corresponding kits. **G.** The ROS level in podocytes was detected by a kit and the results were displayed by flow cytometry. Flow cytometry (**H**) and TUNEL (**I**) were used to evaluate the cell apoptosis of NG-induced podocytes and HG-induced podocytes transfected with sh-NC and sh-DDX3Y. * $p < 0.05$, ** $p < 0.01$, *** $p < 0.001$.

examined by Western blot (Fig. 1F). Consequently, DDX3Y was highly expressed in the blood of DN patients and HG-induced podocytes. This parallel up-regulation across different models underscores DDX3Y's potential significance in the pathophysiology of DN, considering the known link between podocyte injury *in vitro* and systemic manifestations in DN patients.

Knockdown of DDX3Y alleviated HG-induced inflammation, oxidative stress and apoptosis in podocytes

To validate the role of DDX3Y in HG-induced podocytes, the loss-of-function assays were carried out and podocytes were transfected with sh-DDX3Y#1/2/3 and sh-NC. Western blot was first applied for verification of transfection efficiency. The knockdown efficiency of sh-DDX3Y#2 was the most remarkable (Fig. S1A, Supplementary material), so sh-DDX3Y#2 was used as sh-DDX3Y. DDX3Y expression was declined by sh-DDX3Y, which indicated that the transfection was accomplished (Fig. 2A). Likewise, the expression levels of DDX3Y in podocytes treated with different conditions were analyzed using Western blot. HG induction led to an increase in the expression level of DDX3Y. However, with the knockdown of DDX3Y, its expression level in HG-induced podocytes was downregulated (Fig. 2B). Furthermore, cell viability was detected by CCK-8 assay, the reduction in cell viability due to HG induction was reversed by the knockdown of DDX3Y (Fig. S1B and 2C). Then, the levels of inflammatory factors including IL-1β, TNF-α and IL-6 in podocytes were measured using different kits. The results indicated increased levels of inflammatory factors due to HG treatment, with a reduction observed after DDX3Y knockdown (Fig. 2D–F). To further monitor the oxidative stress of podocytes in different groups, the ROS level was detected using a commercial kit. The impact of the elevation of ROS levels in podocytes resulting from HG induction was counteracted by the knockdown of DDX3Y (Fig. 2G). Meanwhile, cell apoptosis was analyzed using both flow cytometry and TUNEL, which suggested that sh-DDX3Y suppressed cell apoptosis in the HG-treated podocytes (Fig. 2H–I). Accordingly, silencing DDX3Y alleviated the reduced cell viability, increased oxidative stress and apoptosis in podocytes induced by HG.

WTAP methylated DDX3Y to promote the stability of DDX3Y mRNA

Subsequently, the regulatory mechanism between WTAP and DDX3Y in DN was investigated. First, the SRAMP database was applied to predict the m6A sites in DDX3Y, which illustrated the presence of m6A methylation sites in DDX3Y (Fig. 3A). Next, the GSE154881 dataset was used to demonstrate the expression levels of three methylated enzymes (METTL3, METTL14 and WTAP) in healthy and DN samples, which illustrated that three of the four DN samples had higher METTL14 and WTAP expression levels than those in the healthy samples (Fig. 3B). Then, the podocytes were transfected with sh-METTL14 and sh-WTAP. Correspondingly, the effects of the methylase (METTL14 and WTAP) on DDX3Y mRNA in HG-induced podocytes were analyzed by qRT-PCR. After the knockdown of METTL14 and WTAP, the mRNA level of DDX3Y in HG-induced podocytes was decreased in both cases. However, the change in the decrease of the DDX3Y mRNA level caused by the knockdown of WTAP was more significant (Fig. 3C). Then, podocytes were treated with sh-WTAP#1/2/3, experimental results showed that WTAP protein in the sh-WTAP#1 and sh-WTAP#2 groups was successfully knocked down, with the knockdown effect of sh-WTAP#1 being statistically extremely significant (Fig. S1C). Additionally, sh-WTAP#1 exhibited the most remarkable restoring effect on HG-induced reduction of podocyte viability (Fig. S1D). Therefore, sh-WTAP#1 was applied in subsequent experiments and labeled as sh-WTAP. The expression level of DDX3Y in HG-induced podocytes was determined by Western blot (Fig. 3D). Next, the m6A level of DDX3Y mRNA was detected using MeRIP assay, in the HG group, m6A level was higher compared to the NC group, however, when WTAP was knockdown, the m6A level of DDX3Y mRNA was significantly decreased (Fig. 3E). Then, DDX3Y mRNA stability was examined by using actinomycin D and qRT-PCR assay. The results demonstrated that sh-WTAP remarkably accelerated the degradation of DDX3Y mRNA caused by actinomycin D in HG-induced podocytes (Fig. 3F). Besides, WTAP mRNA levels in 36 healthy individuals and 32 DN patients were analyzed, as shown in Figure 3G, WTAP mRNA levels in the DN group were higher than that in the control group. Next, an ROC curve was created to evaluate the diagnostic value of WTAP, with a cut off value of 1.245 (Fig. 3H). In addition, the expression levels of WTAP mRNA and DDX3Y mRNA showed a positive correlation (Fig. 3I). Finally, the WTAP protein levels in the NG group and the HG group were monitored by Western blot, which proved that WTAP protein was highly expressed in HG-induced podocytes (Fig. 3J). Collectively, WTAP was highly expressed in podocytes and modified DDX3Y mRNA by m6A modification and was able to stabilize DDX3Y mRNA in this manner.

WTAP promoted HG-induced cell injury in podocytes by regulating DDX3Y

To further validate the regulatory relationship between WTAP and DDX3Y, podocytes were transfected with sh-WTAP and oe-DDX3Y. Western blot was utilized to examine the protein level of DDX3Y in cells treated in different ways.

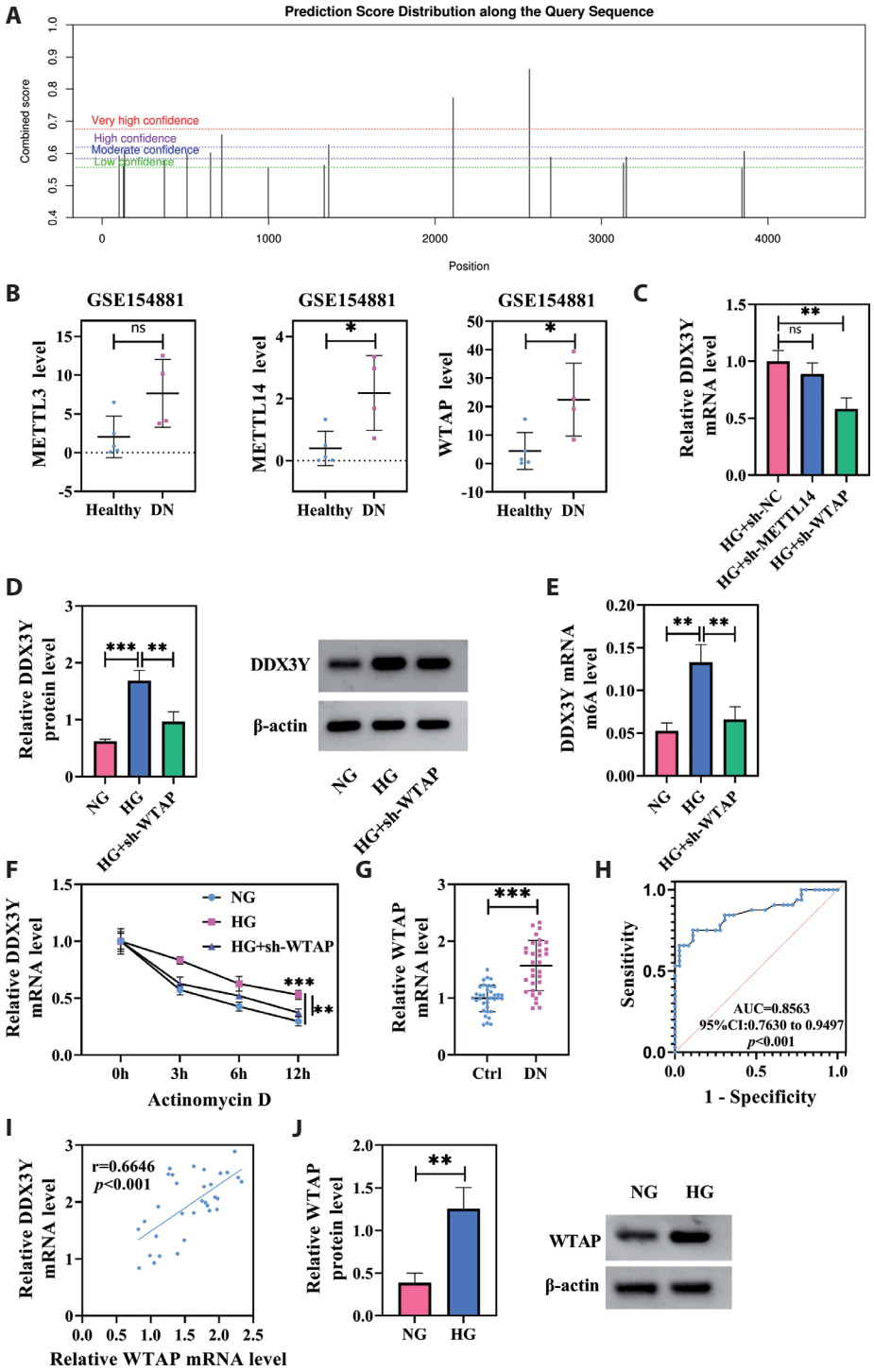

Figure 3. WTAP positively regulates DDX3Y expression through m6A modification. **A.** SRAMP was utilized to predict the m6A sites in DDX3Y. **B.** The GSE154881 dataset showed the expression of three methylases (METTL3, METTL14 and WTAP) in five healthy samples and four samples from patients with DN. **C.** qRT-PCR was used to detect DDX3Y mRNA levels in podocytes transfected with sh-NC, sh-METTL14, and sh-WTAP. **D.** DDX3Y protein expression levels in the HG group and the HG+sh-WTAP group were detected by Western blot. **E.** qRT-PCR assay was applied to measure the DDX3Y mRNA level in podocytes. **F.** Actinomycin D assay for DDX3Y mRNA stability. **G.** WTAP mRNA levels in the samples from 36 healthy volunteers (Ctrl) and DN patients were detected by qRT-PCR assay. **H.** ROC curve analyzed for diagnostic value (cut-off value = 1.245). **I.** Correlation curve between DDX3Y and WTAP (r = 0.6646, $p < 0.001$). **J.** Western blot was used to determine the WTAP protein expression level in podocytes. * $p < 0.05$, ** $p < 0.01$, *** $p < 0.001$.

The results shown in Figure 4A suggested that the transfection was successfully completed. The expression of DDX3Y in the HG+sh-WTAP group was lower than that in the HG+sh-WTAP+oe-DDX3Y group, which demonstrated that WTAP knockdown inhibited the expression of DDX3Y (Fig. 4B). Cell viability was detected by CCK-8 assay. It was found that increased cell viability due to sh-WTAP was reversed by oe-DDX3Y (Fig. 4C). Likewise, the release of downstream pro-inflammatory cytokines (IL-1β, TNF-α and IL-6) and the level of ROS in podocytes were measured by related kits. The inflammatory response and oxidative stress caused by HG induction were mitigated by sh-WTAP. However, these mitigating effects were reversed by DDX3Y overexpression (Fig. 4D–G). Meanwhile, the cell apoptosis was analyzed by flow cytometry and TUNEL, the effects of sh-WTAP and oe-DDX3Y on apoptosis were similar to the above results (Fig. 4H,I). As a result, WTAP exacerbated HG-induced inflammation, oxidative stress and apoptosis in podocytes by targeting DDX3Y.

The alleviating effect of WTAP knockdown on renal injury was reversed by DDX3Y overexpression

db/db mice were utilized to establish the *in vivo* model of DN. In order to observe the pathological changes in the renal tissues in each group, the renal tissues of mice were stained with HE and PAS, the results were displayed in Figure 5A. The db/db group showed manifestations of renal injury such as glomerular enlargement, increased extracellular matrix (ECM), tubular dilation, and basement membrane thickening. The renal injury in the db/db+sh-WTAP group was alleviated, with reduced ECM proliferation and less severe basement membrane thickening. However, the renal injury in the db/db+sh-WTAP+oe-DDX3Y group returned to a level close to that of the db/db group, indicating that DDX3Y overexpression reversed the alleviating effect of WTAP knockdown on renal injury. Then, the serum BUN, serum Scr, urine protein and inflammatory factors were measured. Compared with db/m mice, these indicators were high in the serum of db/db mice, illustrating kidney damage and impaired kidney functions. However, these indices were significantly reduced in mice treated with sh-WTAP, and these effects were restored by oe-DDX3Y (Fig. 5B–G). Subsequently, the cell apoptosis in renal cells was analyzed by TUNEL, and sh-WTAP inhibited cell apoptosis induced by DN, but DDX3Y overexpression mitigated this effect (Fig. 5H). In addition, the expression levels of WTAP and DDX3Y were respectively analyzed by Western blot, indicating that sh-WTAP decreased the DDX3Y expression. On the contrary, oe-DDX3Y had no effects on the expression of WTAP (Fig. 5I). All results above suggested that WTAP promoted renal insufficiency and histopathological alterations in diabetic mice by regulating DDX3Y expression.

Discussion

The prevalence of DN has been increasing annually and has overtaken primary glomerular disease as the primary cause of chronic renal disease (Zhang and Kong 2020). It is not only hazardous to the health of Chinese residents, but also seriously affects China's socio-economic development (Duan et al. 2019). Therefore, understanding the mechanisms of disease and discovering more therapeutic targets was particularly urgent for the current situation. In our current study, the GEO database was applied, and DDX3Y was found to be upregulated in the blood of DN patients. A previous study has clarified that DDX3Y-induced cigarette smoke extract-induced human bronchial epithelial cell injury by modulating toll-like receptor 4 (TLR4)/NF-κB pathway (Jia and Zhao 2020). Podocytes injury was a crucial factor in the pathogenesis of DN (Li et al. 2023). Nevertheless, the function of DDX3Y in HG-induced podocyte damage was unclear yet, so our subsequent studies were therefore dedicated to exploring the effects of DDX3Y on HG-induced podocytes. In addition to bioinformatics predictions, qRT-PCR and Western blot illustrated that DDX3Y was highly expressed in DN and HG-induced podocytes. Besides, the knockdown of DDX3Y inhibited inflammatory responses, oxidative stress and apoptosis in podocytes due to HG induction. Given the central role of DDX3Y in the context of DN-related podocyte function, we then turned our attention to the potential molecular mechanisms underlying these processes.

As the most common form of mRNA modification in mammals, m6A modification is recognized for its significant involvement in multiple biological processes and its contribution to the onset of various diseases (Uddin et al. 2021; Song et al. 2022). Li et al. (2021) demonstrated that METTL14 mediated alpha-klotho *via* m6A modification to promote the glomerular endothelial cell damage and DN. Additionally, a study has found that podocyte injury was promoted due to METTL3 modifying TIMP mRNA in an m6A manner (Jiang et al. 2022). In the current work, SRAMP was utilized for the prediction of m6A sites in DDX3Y. Unexpectedly, DDX3Y mRNA had m6A sites. METTL14 and WTAP expression were found to be upregulated in three of the four DN patient samples. Moreover, we explored the effects of methylases (METTL14 and WTAP) on DDX3Y mRNA in injured podocytes. The results suggested that sh-WTAP had the greatest effect on DDX3Y mRNA expression in HG-induced podocytes. A recent study has proved that WTAP promoted renal injury in DN by modifying NLRP3 in an m6A manner (Lan et al. 2022). Therefore, we were even more interested in knowing whether WTAP regulation of DDX3Y plays a role in injured podocytes.

WTAP is one of the key components of the m6A methyltransferase complex *in vivo*, and its role in DN and related

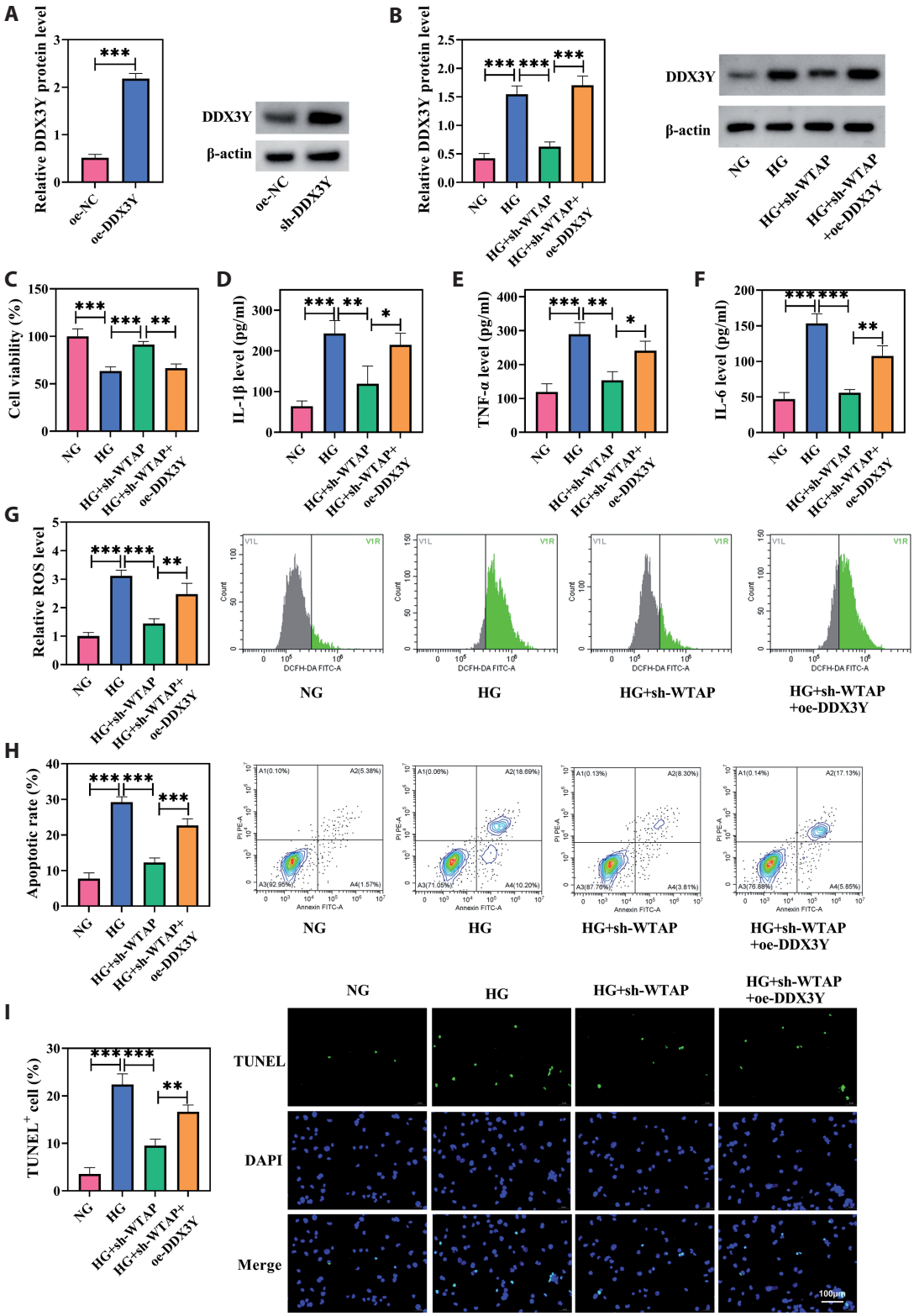

Figure 4. WTAP/DDX3Y promotes HG-induced inflammation, oxidative stress and apoptosis in podocytes. HG-induced podocytes were transfected with sh-WTAP, sh-WTAP+oe-SSX3Y. **A,B.** Western blot was applied to determine the DDX3Y protein expression level in podocytes. **C.** Cell viability was detected by CCK-8 assay. The levels of inflammatory factors IL-1β (**D**), TNF-α (**E**), and IL-6 (**F**), and ROS (**G**) in podocytes were detected using commercial kits. Cell apoptosis was detected by flow cytometry (**H**) and TUNEL (**I**). $^{*}p < 0.05$, $^{**}p < 0.01$, $^{***}p < 0.001$.

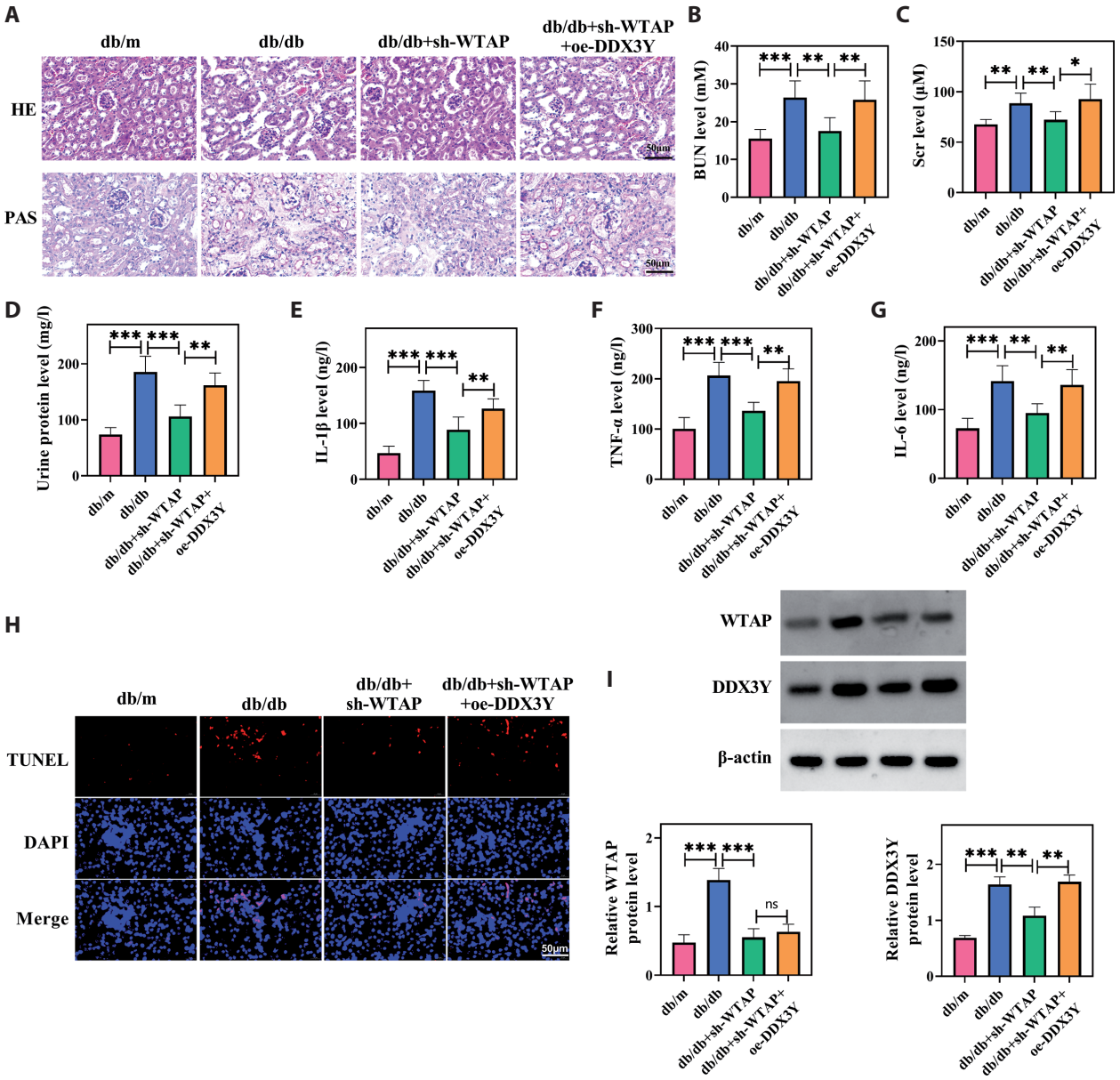

Figure 5. WTAP/DDX3Y promotes renal insufficiency and histopathological changes in diabetic mice. **A.** Renal tissue morphology of mice in different groups was demonstrated using HE and PAS staining. The levels of BUN (**B**) and Scr (**C**) in serum and Urine protein (**D**) were measured using corresponding kits. The levels of IL-1β (**E**), TNF-α (**F**) and IL-6 (**G**) were detected using commercial kits. **H.** Cell viability was detected by TUNEL. **I.** The protein expression levels of WTAP and DDX3Y were determined by Western blot. * $p < 0.05$, ** $p < 0.01$, *** $p < 0.001$.

regulatory mechanisms has been uncovered by many studies (Bai and Huang 2024; Zhang et al. 2024). In our present work, the effect of WTAP on DDX3Y expression in podocytes was explored, in which, sh-WTAP suppressed DDX3Y expression in HG-induced podocytes. In addition, the MeRIP assay was applied to assess the effects of WTAP on the level of m6A modification in DDX3Y mRNA. It could be concluded that WTAP modified DDX3Y mRNA by m6A and stabilized DDX3Y mRNA in this manner. Based on the *in vivo* and *in vitro* experiments, the conclusion could be summarized: WTAP promoted high glucose-induced inflammation, oxidative stress and apoptosis in podocytes through DDX3Y, and also promoted renal insufficiency and histopathological changes in diabetic mice.

As can be seen, WTAP contributed to the injury of podocytes both *in vivo* and *in vitro*. The roles of the regulatory

mechanism that exists between WTAP and DDX3Y for DN cell injury were illustrated in our work. In a word, WTAP regulated the m6A modification and stability of DDX3Y mRNA to exacerbate the renal injury in DN, uncovering a novel molecular mechanism of WTAP in podocyte injury and DN, which provides another new target and understanding for DN pathogenesis and disease treatment. However, this study has limitations. The sample size in clinical experiments was relatively small, and the cell lines used *in vitro* deviated from the *in vivo* podocyte environment. Also, the complexity of the DN network might have been oversimplified, and the animal model did not fully mimic human DN. Looking ahead, future research should focus on expanding sample sizes, using more physiologically relevant models, and comprehensively exploring related molecular mechanisms to further validate and expand on these findings, aiming to translate this knowledge into more effective therapeutic strategies for DN patients.

Data availability statement. The data are available from the corresponding author upon reasonable request.

Conflict of interests. The author claims that there is no conflict of interests.

References

Bai Y, Huang L (2024): Marrow mesenchymal stem cell mediates diabetic nephropathy progression via modulation of Smad2/3/WTAP/m6A/ENO1 axis. FASEB J. **38,** e23729 https://doi.org/10.1096/fj.202301773R

Dou X, Huang L, Xiao Y, Liu C, Li Y, Zhang X, Yu L, Zhao R, Yang L, Chen C et al. (2023): METTL14 is a chromatin regulator independent of its RNA N6-methyladenosine methyltransferase activity. Protein Cell **14,** 683-697 https://doi.org/10.1093/procel/pwad009

Duan J, Wang C, Liu D, Qiao Y, Pan S, Jiang D, Zhao Z, Liang L, Tian F, Yu P et al. (2019): Prevalence and risk factors of chronic kidney disease and diabetic kidney disease in Chinese rural residents: a cross-sectional survey. Sci. Rep. **9,** 10408 https://doi.org/10.1038/s41598-019-46857-7

Elendu C, John Okah M, Fiemotongha KDJ, Adeyemo BI, Bassey BN, Omeludike EK, Obidigbo B (2023): Comprehensive advancements in the prevention and treatment of diabetic nephropathy: A narrative review. Medicine (Baltimore) **102,** e35397 https://doi.org/10.1097/MD.0000000000035397

Fu K, Jing C, Shi J, Mao S, Lu R, Yang M, Chen Y, Qian B, Wang Y, Li L (2024): WTAP and METTL14 regulate the m6A modification of DKK3 in renal tubular epithelial cells of diabetic nephropathy. Biochem. Biophys. Res. Commun. **738,** 150524 https://doi.org/10.1016/j.bbrc.2024.150524

He L, Li H, Wu A, Peng Y, Shu G, Yin G (2019): Functions of N6-methyladenosine and its role in cancer. Mol. Cancer **18,** 176 https://doi.org/10.1186/s12943-019-1109-9

Horiuchi K, Kawamura T, Hamakubo T (2021): Wilms' tumor 1-associating protein complex regulates alternative splicing and polyadenylation at potential G-quadruplex-forming splice site sequences. J. Biol. Chem. **297,** 101248 https://doi.org/10.1016/j.jbc.2021.101248

Huang H, Weng H, Chen J (2020): The biogenesis and precise control of RNA m(6)A methylation. Trends Genet. **36,** 44-52 https://doi.org/10.1016/j.tig.2019.10.011

Jia R, Zhao XF (2020): MicroRNA-497 functions as an inflammatory suppressor via targeting DDX3Y and modulating toll-like receptor 4/NF-κB in cigarette smoke extract-stimulated human bronchial epithelial cells. J. Gene Med. **22,** e3137 https://doi.org/10.1002/jgm.3137

Jiang L, Liu X, Hu X, Gao L, Zeng H, Wang X, Huang Y, Zhu W, Wang J, Wen J et al. (2022): METTL3-mediated m(6)A modification of TIMP2 mRNA promotes podocyte injury in diabetic nephropathy. Mol. Ther. **30,** 1721-1740 https://doi.org/10.1016/j.ymthe.2022.01.002

Jiang X, Liu B, Nie Z, Duan L, Xiong Q, Jin Z, Yang C, Chen Y (2021): The role of m6A modification in the biological functions and diseases. Signal Transduct. Target Ther. **6,** 74 https://doi.org/10.1038/s41392-020-00450-x

Lacroix M, Beauchemin H, Khandanpour C, Möröy T (2023): The RNA helicase DDX3 and its role in c-MYC driven germinal center-derived B-cell lymphoma. Front. Oncol. **13,** 1148936 https://doi.org/10.3389/fonc.2023.1148936

Lan J, Xu B, Shi X, Pan Q, Tao Q (2022): WTAP-mediated N(6)-methyladenosine modification of NLRP3 mRNA in kidney injury of diabetic nephropathy. Cell Mol. Biol. Lett. **27,** 51 https://doi.org/10.1186/s11658-022-00350-8

Li C, Su F, Liang Z, Zhang L, Liu F, Fan W, Li Z (2022): Macrophage M1 regulatory diabetic nephropathy is mediated by m6A methylation modification of lncRNA expression. Mol. Immunol. **144,** 16-25 https://doi.org/10.1016/j.molimm.2022.02.008

Li M, Deng L, Xu G (2021): METTL14 promotes glomerular endothelial cell injury and diabetic nephropathy via m6A modification of α-klotho. Mol. Med. **27,** 106 https://doi.org/10.1186/s10020-021-00365-5

Li S, Feng T, Yuan H, Li Q, Zhao G, Li K (2024): DEAD-box RNA helicases in the multistep process of tumor metastasis. Mol. Biol. Rep. **51,** 1006 https://doi.org/10.1007/s11033-024-09912-9

Li X, Zhang Y, Xing X, Li M, Liu Y, Xu A, Zhang J (2023): Podocyte injury of diabetic nephropathy: Novel mechanism discovery and therapeutic prospects. Biomed. Pharmacother. **168,** 115670 https://doi.org/10.1016/j.biopha.2023.115670

Qin Y, Wu S, Zhang F, Zhou X, You C, Tan F (2023): N6-methyladenosine methylation regulator RBM15 promotes the progression of diabetic nephropathy by regulating cell proliferation, inflammation, oxidative stress, and pyroptosis through activating the AGE-RAGE pathway. Environ. Toxicol. **38,** 2772-2782 https://doi.org/10.1002/tox.23917

Qiu Y, Tang J, Zhao Q, Jiang Y, Liu YN (2023): From diabetic nephropathy to end-stage renal disease: The Effect of chemokines on the immune system. J. Diabetes Res. **2023,** 3931043 https://doi.org/10.1155/2023/3931043

Queeley GL, Campbell ES (2018): Comparing treatment modalities for end-stage renal disease: A meta-analysis. Am. Health Drug Benefits **11,** 118-127

Sagoo MK, Gnudi L (2020): Diabetic nephropathy: An overview. Methods Mol. Biol. **2067,** 3-7
https://doi.org/10.1007/978-1-4939-9841-8_1

Samsu N (2021): Diabetic Nephropathy: Challenges in pathogenesis, diagnosis, and treatment. Biomed. Res. Int. **2021,** 1497449
https://doi.org/10.1155/2021/1497449

Song N, Cui K, Zhang K, Yang J, Liu J, Miao Z, Zhao F, Meng H, Chen L, Chen C et al. (2022): The role of m6A RNA methylation in cancer: Implication for nature products anti-cancer research. Front. Pharmacol. **13,** 933332
https://doi.org/10.3389/fphar.2022.933332

Su R, Dong L, Li Y, Gao M, He PC, Liu W, Wei J, Zhao Z, Gao L, Han L et al. (2022): METTL16 exerts an m6A-independent function to facilitate translation and tumorigenesis. Nat. Cell Biol. **24,** 205-216
https://doi.org/10.1038/s41556-021-00835-2

Uddin MB, Wang Z, Yang C (2021): The m(6)A RNA methylation regulates oncogenic signaling pathways driving cell malignant transformation and carcinogenesis. Mol. Cancer **20,** 61
https://doi.org/10.1186/s12943-021-01356-0

Wu S, Sun X, Hua R, Hu C, Qin L (2024): DDX21 functions as a potential novel oncopromoter in pancreatic ductal adenocarcinoma: a comprehensive analysis of the DExD box family. Discov. Oncol. **15,** 333
https://doi.org/10.1007/s12672-024-01204-9

Zeng C, Huang W (2020): Roles of METTL3 in cancer: mechanisms and therapeutic targeting. J. Hematol. Oncol. **13,** 117
https://doi.org/10.1186/s13045-020-00951-w

Zhang L, Wen Z, Han L (2020): Research progress on the pathological mechanisms of podocytes in diabetic nephropathy. J. Diabetes Res. **2020,** 7504798
https://doi.org/10.1155/2020/7504798

Zhang W, Qian Y, Jia G (2021): The detection and functions of RNA modification m(6)A based on m(6)A writers and erasers. J. Biol. Chem. **297,** 100973
https://doi.org/10.1016/j.jbc.2021.100973

Zhang XX, Kong J (2020): Prevalence of diabetic nephropathy among patients with type 2 diabetes mellitus in China: A meta-analysis of observational studies. J. Diabetes Res. **2020,** 2315607
https://doi.org/10.1155/2020/2315607

Zhang Z, Zhou F, Lu M, Zhang D, Zhang X, Xu S, He Y (2024): WTAP-mediated m(6)A modification of TRIM22 promotes diabetic nephropathy by inducing mitochondrial dysfunction via ubiquitination of OPA1. Redox. Rep. **29,** 2404794
https://doi.org/10.1080/13510002.2024.2404794

Received: January 16, 2025
Final version accepted: April 10, 2025